Supporting Information for

Bioinspired Suprahelical Frameworks as Scaffolds for Artificial Photosynthesis

Kai Tao[*,⊤,†], *Bin Xue*[*,§,†], *Shuyi Han*[∥], *Ruth Aizen*[‡], *Linda J. W. Shimon*[&], *Zhengyu Xu*[§], *Yi Cao*[§], *Deqing Mei*[⊤], *Wei Wang*[§], *Ehud Gazit*[*,‡]

[⊤] State Key Laboratory of Fluid Power and Mechatronic Systems & Key Laboratory of Advanced Manufacturing Engineering of Zhejiang Province, School of Mechanical Engineering, Zhejiang University, Hangzhou 310027, China.

[§] National Laboratory of Solid State Microstructure, Department of Physics, Nanjing University, 22 Hankou Road, Nanjing 210093, Jiangsu, China.

[‡] School of Molecular Cell Biology and Biotechnology, George S. Wise Faculty of Life Sciences, Tel Aviv University, 6997801, Tel Aviv, Israel.

[∥] China Petroleum Engineering & Construction Corp. Southwest Company, No. 6th Shenghua Road, High-Tech Zone, Chengdu 610094, Sichuan, China.

[&] Department of Chemical Research Support, Weizmann Institute of Science, Rehovot 7610001, Israel.

Corresponding Author

[*] E-mail: ehudg@post.tau.ac.il, kai.tao@zju.edu.cn, xuebinnju@nju.edu.cn

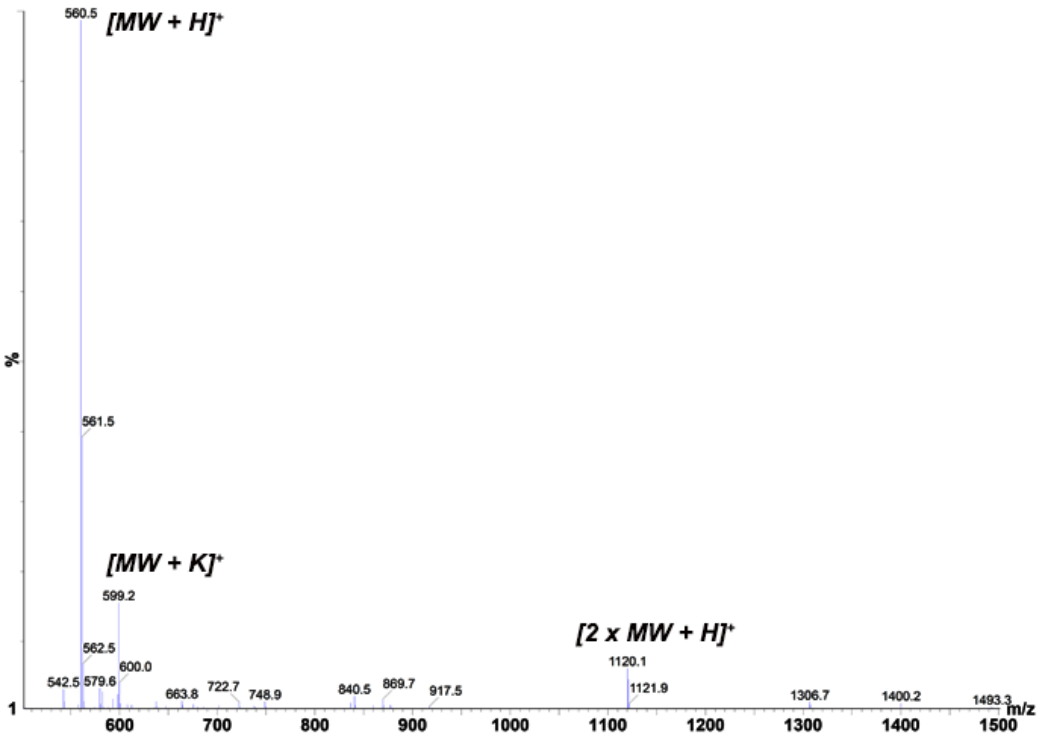

Figure S1. MS spectrum of the synthesized diPNA-**GC**. The observed molecular masses are consistent with the calculated ones, demonstrating the identity of the diPNA sample:

Expected masses $[MW + H]^+$=560.55, $[MW + K]^+$=597.55, $[2 X MW + H]^+$=1120.10;

Observed masses $[MW + H]^+$=560.5, $[MW + K]^+$= 599.2, $[2 X MW + H]^+$=1120.1.

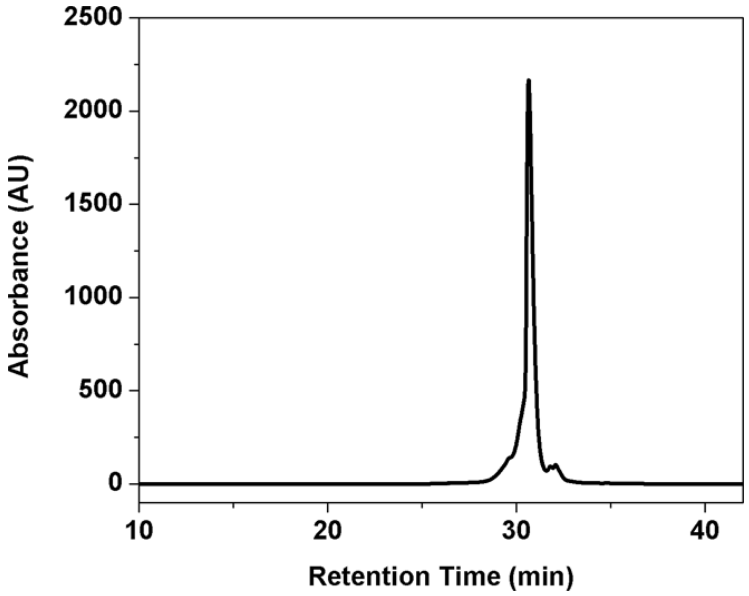

Figure S2. Reversed phase HPLC profile of the synthesized diPNA-**GC**. The monitoring wavelength was set at 214 nm, and the flow rate was 1 mL min^{-1}.

The diPNA peak highly dominates the profile with a relative area of more than 95%, indicating the high purity of the synthesized compound.

Table S1. Dipeptide/diPNA sequences examined in this work and their crystal structure parameters

Dipeptide/diPNA sequence	Crystal parameters	CCDC
FF[1]	*P* 6_1 - hexagonal a=b=24.1600 Å c=5.4590 Å V=2759.55 Å^3 Z=6	
VV	*P* 6_1 - hexagonal a=b=14.5247(1) Å c=10.3176(1) Å V=1885.05(4) Å^3 Z=6	1939394
FV	*P* $2_12_12_1$ - orthorhombic a=5.0788(0) Å b=13.2003(1) Å c=20.0637(1) Å V=1345.09(1) Å^3 Z=4	1939402
FI	*P* 2_1 - monoclinic a=5.5613(1) Å b=17.0408(1) Å c=16.6101(1) Å β=96.560(1)° V=1563.82(3) Å^3 Z=4	1939405
LV	*P* 6_2 - hexagonal a=b=29.1045(3) Å c=11.6866(2) Å V=8573.12(23) Å^3 Z=6	1939406
IV	*P* 6_1 - hexagonal a=b=14.8051(1) Å c=10.2768(1) Å V=1950.79(2) Å^3 Z=6	1939407
LI	*P* 2_12_12 - orthorhombic a=11.2396(1) Å b=28.9560(2) Å c=13.9683(1) Å V=4546.04(5) Å^3 Z=4	1939408
diPNA-**GC**	P 1 - triclinic a=20.5001 Å b=20.5003 Å c=17.4465 Å α=106.5667° β=106.5666° γ=63.0753° V=6160.60 Å^3	1939620

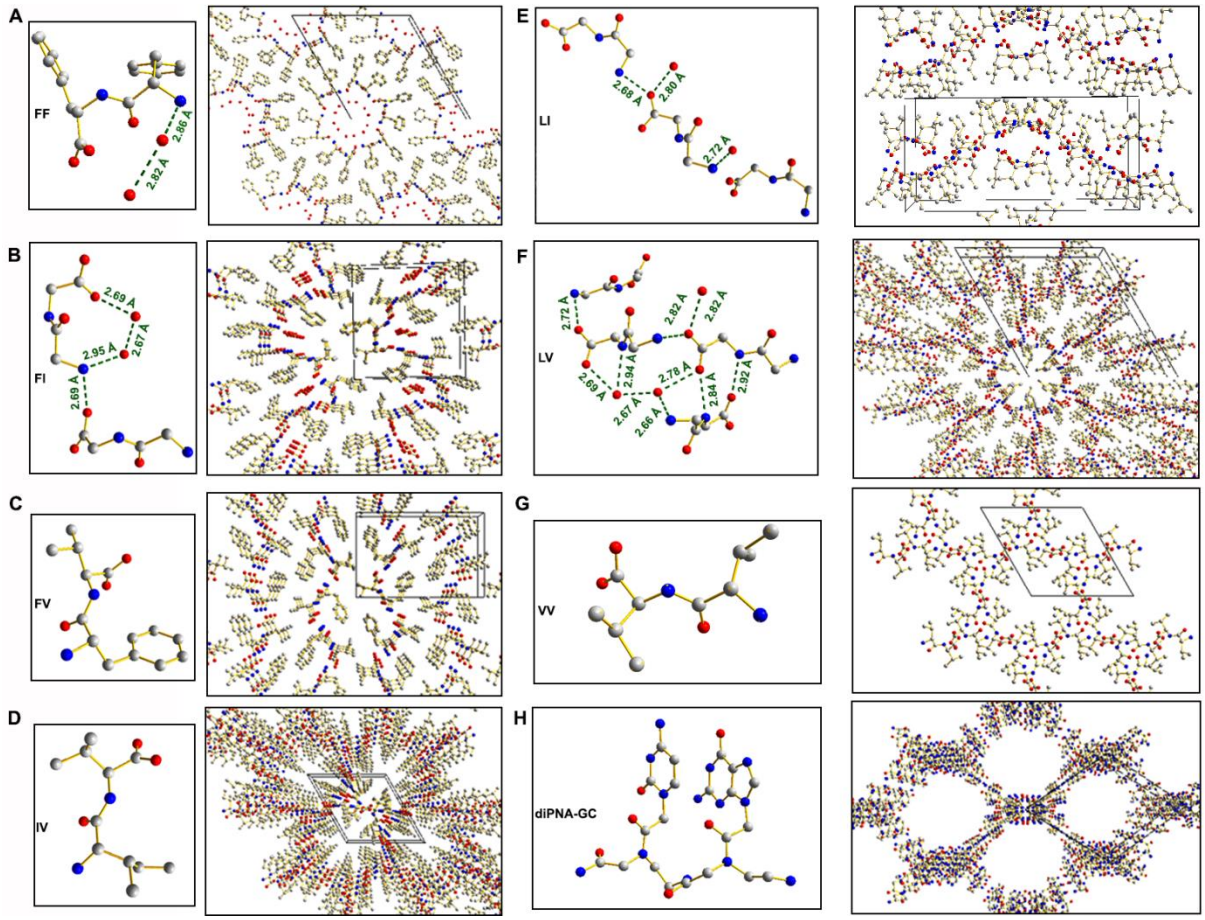

Figure S3. Crystallographic structures of the dipeptides and diPNA crystals detailed in Table S1. (A) **FF**. (B) **FI**. (C) **FV**. (D) **IV**. (E) **LI**. (F) **LV**. (G) **VV**. (H) diPNA-**GC**. In each item, the left panel presents the monomeric molecular structure, with or without co-crystallized water molecule(s). The right panel shows the comprehensive structure of the crystal, demonstrating the distinct organization architectures. The black frameworks show the unit cell in every crystal structure. The carbon, oxygen and nitrogen atoms are designated in grey, red and blue, respectively; the hydrogen atoms are neglected for clarity. The hydrogen bonds between the donor and acceptor atoms are labelled in green dotted lines, with the bond length values labelled in the corresponding locations.

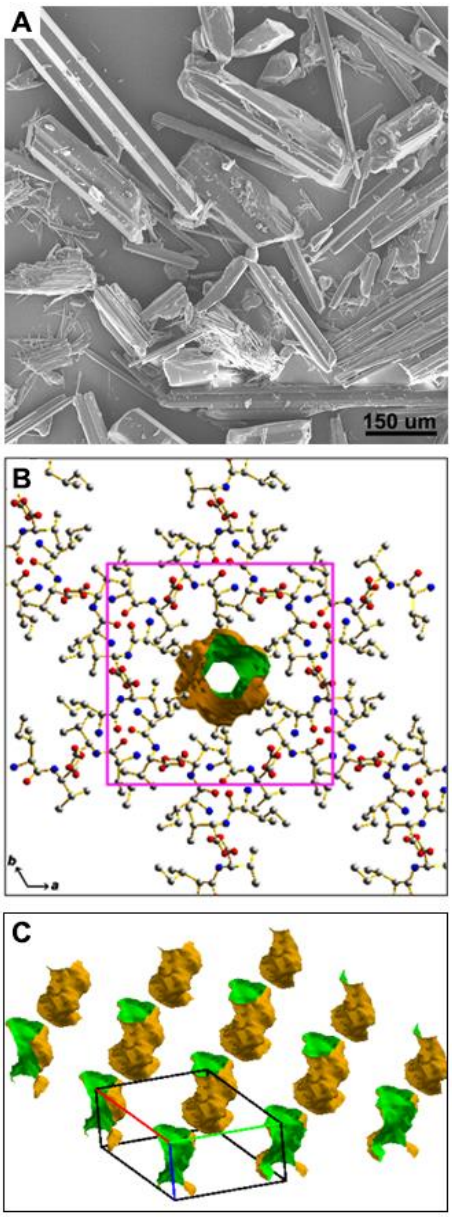

Figure S4. Morphological and cavity characterization of the supramolecular frameworks assembled by **IV**. (A) SEM image of the supramolecular frameworks. (B) Crystallographic image showing the molecular structures comprising the cavities. The magenta framework indicates the suprahelical architecture. The coloured graphic denotes the channel inside the frameworks. The carbon, oxygen and nitrogen atoms are designated in grey, red and blue, respectively; the hydrogen atoms are neglected for clarity. (C) Schematic cartoon showing the array of channels inside the frameworks. The hexahedron represents the unit cell axes of the crystal.

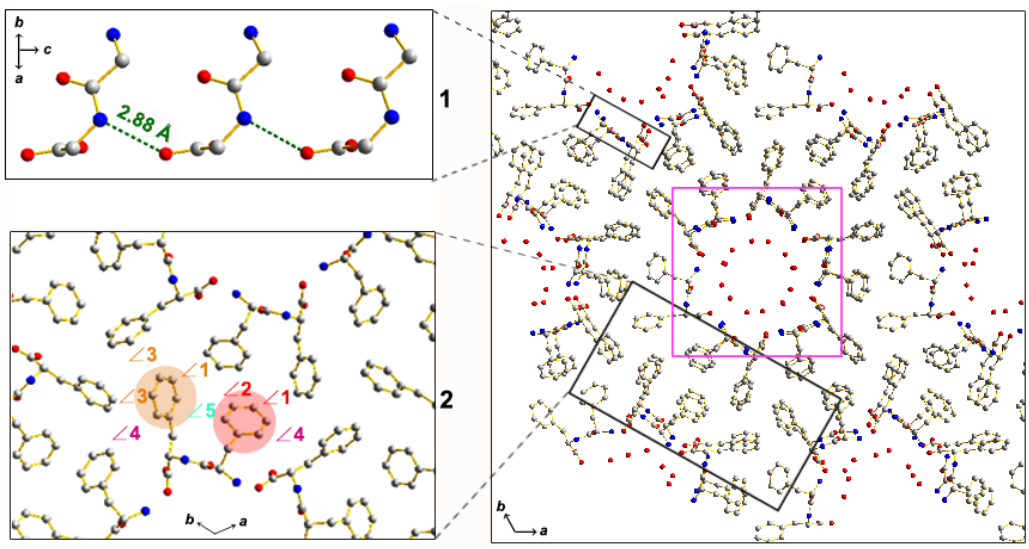

Figure S5. Crystallographic packing of **FF** self-assembling frameworks. Right panel: Comprehensive presentation showing the packing structures along the *ab* plane, the same as Figure 1E in the main text. The magenta framework indicates the suprahelical architecture. The localized crystal structures are numerically shown on the left side: (**1**) backbone parallel β-sheet hydrogen bonding along the *c* direction; (**2**) aromatic interactions between adjacent cavities along the *ab* plane. The dihedral angles formed by the benzyl side-chain (marked in pink and orange) with neighbouring rings are numerically symbolized. ∠1: 76.7°; ∠2: 86.2°; ∠3: 84.6°; ∠4: 83.6°; ∠5: 61.3°. The carbon, oxygen and nitrogen atoms are designated in grey, red and blue, respectively; the hydrogen atoms are neglected for clarity. The hydrogen bonds between the donor and acceptor atoms are labelled in green dotted lines, with the bond length values labelled in the corresponding positions.

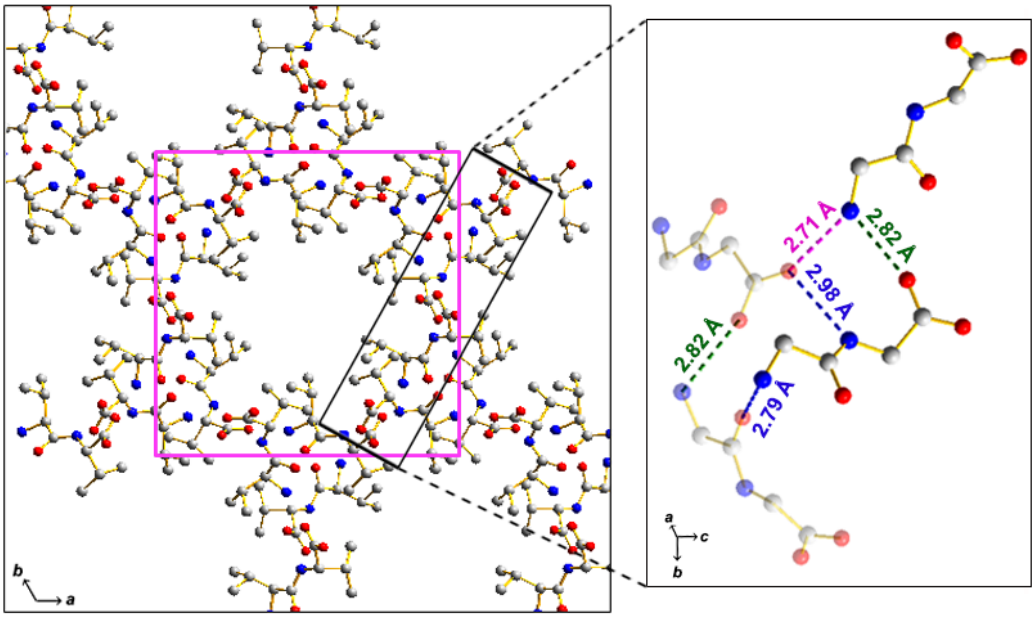

Figure S6. Molecular structures of **VV** assembling frameworks. Left panel: Comprehensive display showing the packing structures along the *ab* plane, the same as Figure 1F in the main text. The magenta framework indicates the suprahelical architecture. The hydrogen bonding interactions between adjacent suprahelices are magnified in the right panel. The carbon, oxygen and nitrogen atoms are designated in grey, red and blue, respectively; the hydrogen atoms are neglected for clarity. The hydrogen bonds composing the suprahelices and connecting the adjacent suprahelices are labelled in green and blue/magenta dotted lines, respectively, with the bond length values labelled in the corresponding colours and positions.

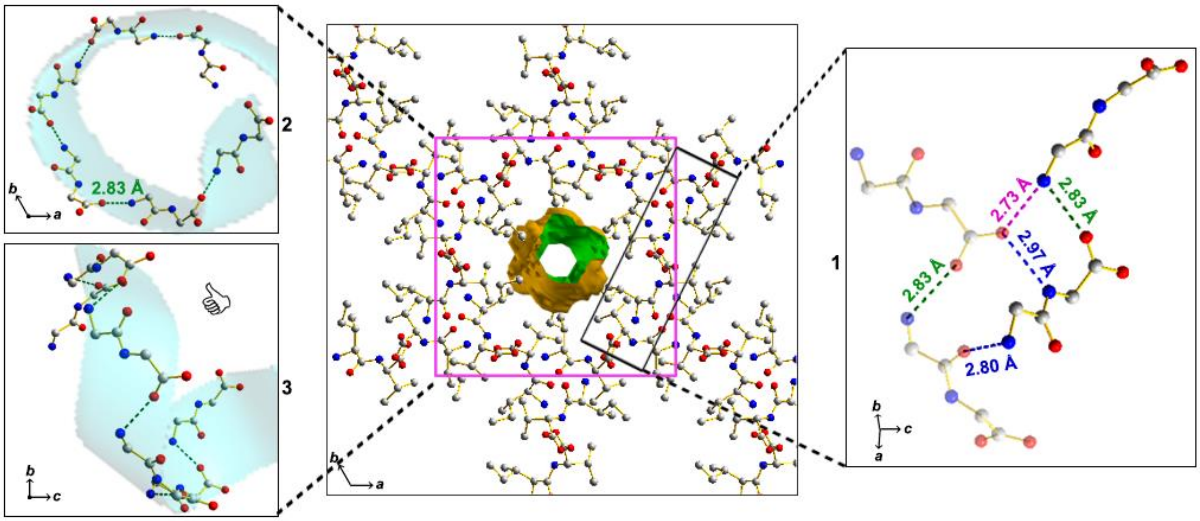

Figure S7. Molecular structures of **IV** assembling frameworks. Central panel: Comprehensive display showing the packing structures along the *ab* plane. The magenta framework indicates the suprahelical architecture. The hydrophobic channel is marked with a coloured cartoon. Magnified crystal structures are numerically shown on either side and labelled in the central panel. Specifically, the hydrogen bonding interactions between adjacent helices are marked in (**1**). The hydrogen bonds composing the suprahelices and connecting the adjacent suprahelices are labelled in green and blue/magenta, respectively. (**2, 3**) Detailed presentation of a pitch of **IV** right-handed helix along the *c* direction from (**2**) front view and (**3**) lateral review. The carbon, oxygen and nitrogen atoms are designated in grey, red and blue, respectively; the hydrogen atoms are neglected for clarity. The hydrogen bonds between the donor and acceptor atoms are labelled in dotted lines, with the bond length values labelled in the corresponding colours and locations.

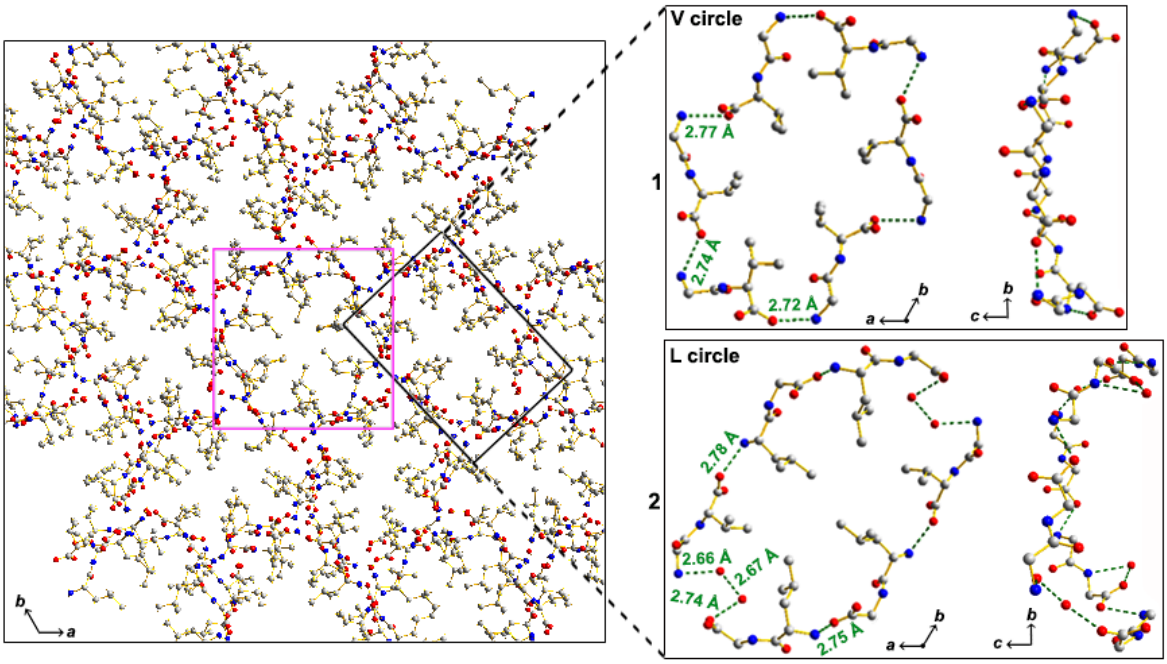

Figure S8. Crystallographic structures of the **LV** supramolecular frameworks. Left panel: Comprehensive view presenting the packing structures along the *ab* plane, showing a larger void surrounded by six smaller ones, as shown in Figure 1G in the main text. The magenta framework indicates the suprahelical architecture. The two alternating supramolecular circles, designated (**1**) "**V** circle" and (**2**) "**L** circle", are magnified from both front and lateral views in the right panels. The carbon, oxygen and nitrogen atoms are designated in grey, red and blue, respectively; the hydrogen atoms are neglected for clarity. The hydrogen bonds between the donor and acceptor atoms are labelled in green dotted lines, with the bond length values labelled in the corresponding positions.

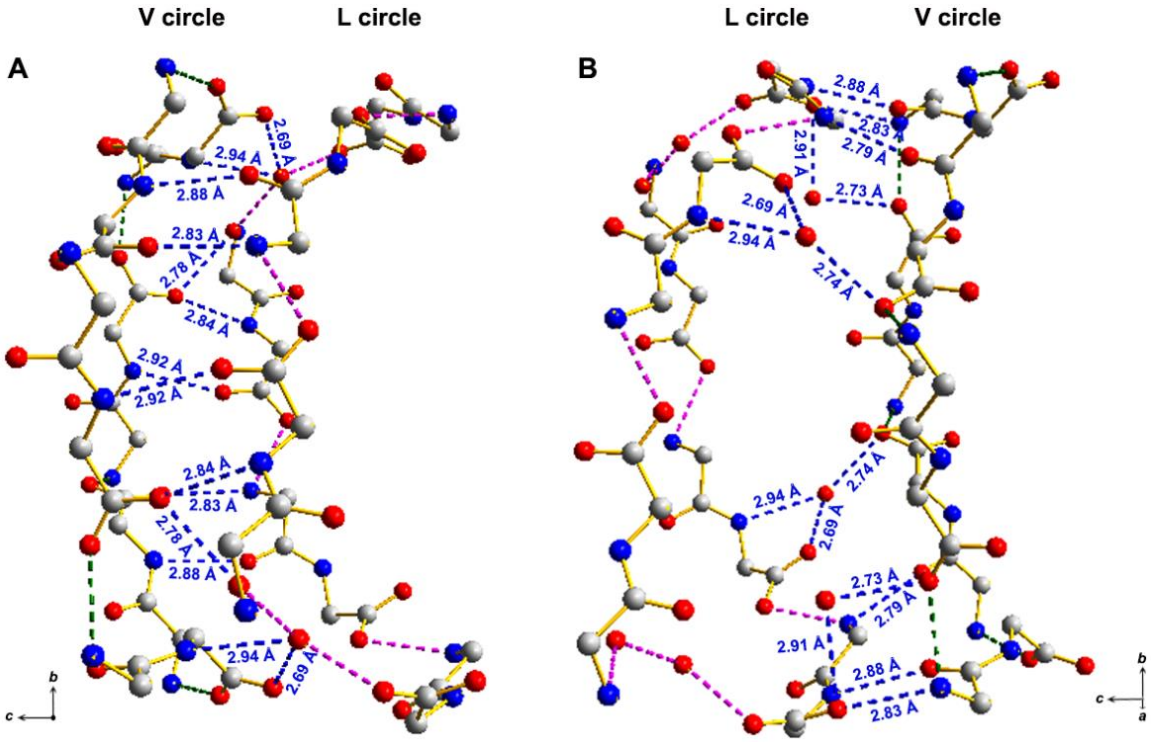

Figure S9. Magnified representation of the hydrogen bonding network between alternating "**V** circle" and "**L** circle" along the *c* direction in **LV** suprahelical frameworks, marked in blue dotted lines with the bond length values labelled in the corresponding positions. (A) **V**-**L**; (B) **L**-**V**. The hydrogen bonds composing the "**V** circle" and "**L** circle" are marked in green and pink dotted lines, respectively. The carbon, oxygen and nitrogen atoms are designated in grey, red and blue, respectively; the hydrogen atoms and side chains are neglected for clarity.

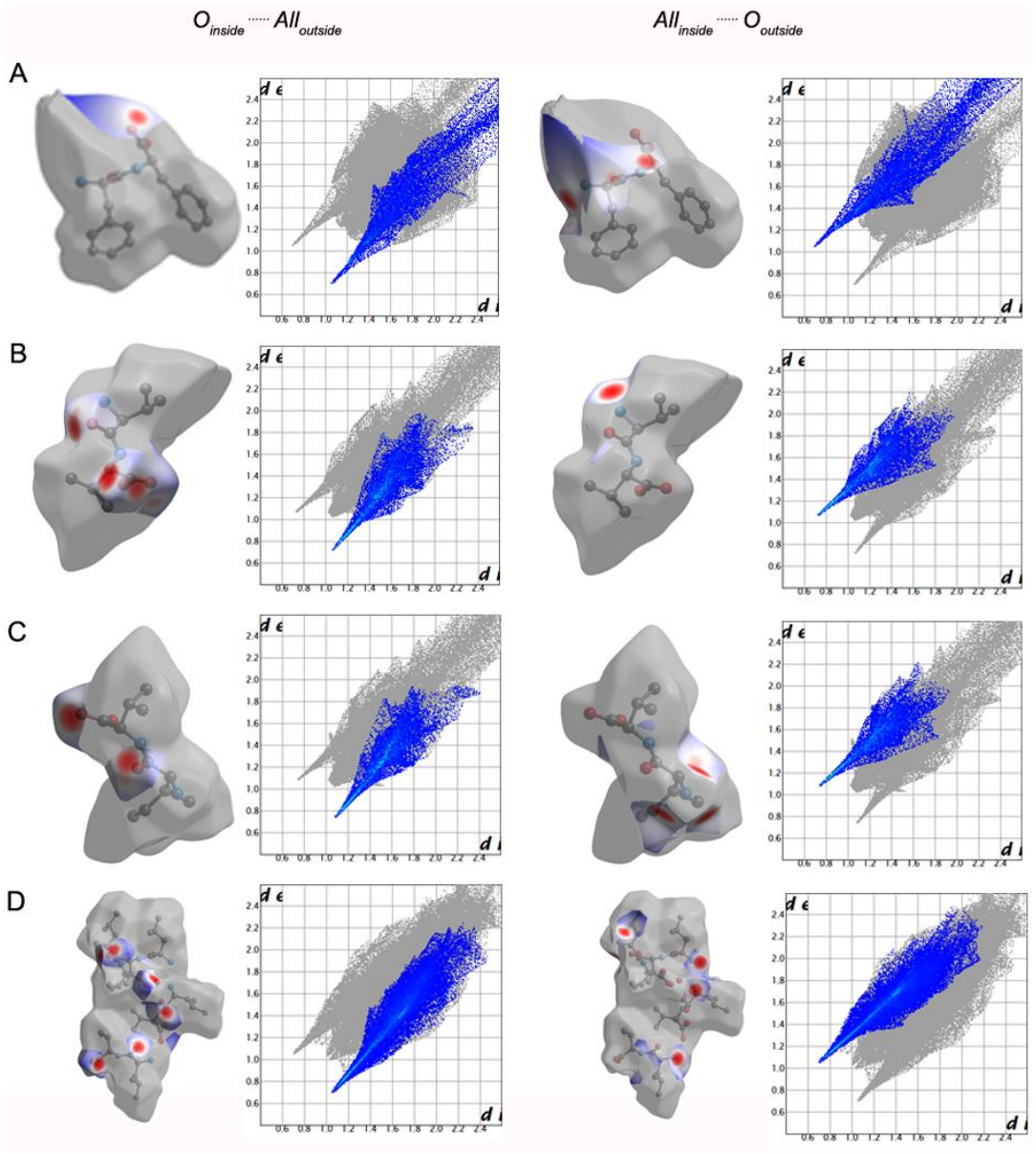

Figure S10. Hirshfeld surface and the 2-D fingerprint plot of the dipeptide-based suprahelical frameworks. (A) **FF**, (B) **VV**, (C) **IV**, (D) **LV**. In each item, the left and right panels show the highlight close contacts of O_{inside}-$All_{outside}$ and All_{inside}-$O_{outside}$, respectively.

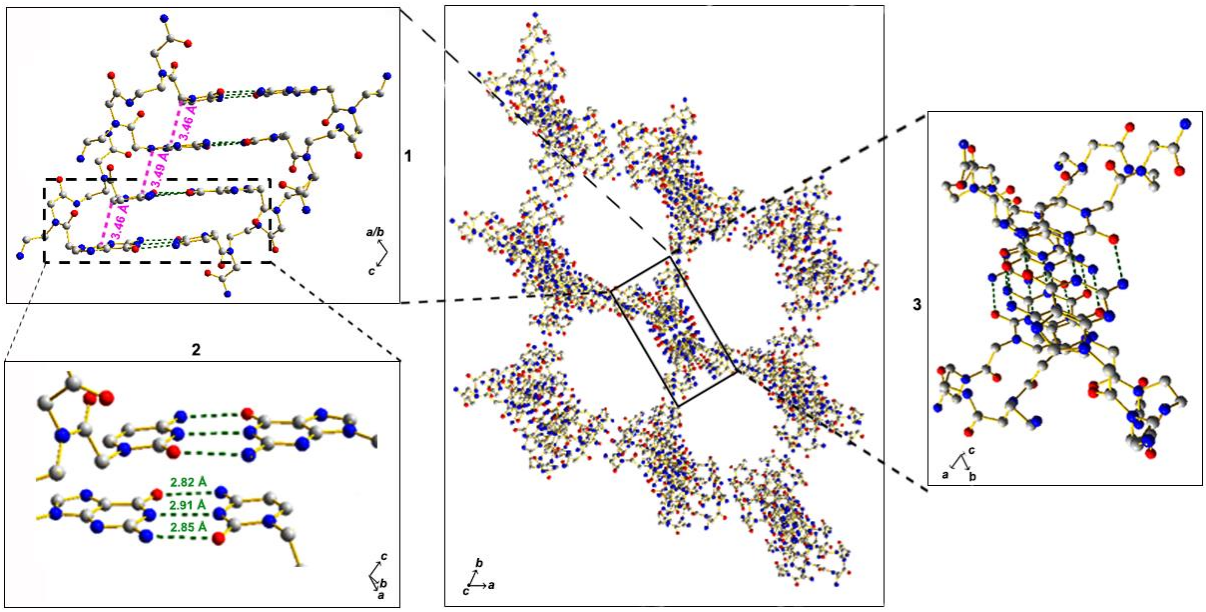

Figure S11. Packing structures of the diPNA-**GC** supramolecular frameworks. Central panel: Schematic presentation showing the channels along the *c* direction, as shown in the upper panel of Figure 1H in the main text. The magnified crystal structures are numerically shown on either side and labelled in the central panel. Specifically, magnified presentations of (**1**) side-view of base stacking along the *c* direction and (**2**) detailed view of the **G**-**C** Watson-Crick hydrogen bonding base pairs are shown. (**3**) Front-view of the base stacking along the *c* direction in (**1**), showing the different orientation of the four amide backbones, underlying the basis of the porous nature. The hydrogen bonds between the donor and acceptor atoms and the aromatic interactions are labelled in green and magenta dotted lines, respectively, with the bond length values labelled in the corresponding colours and positions.

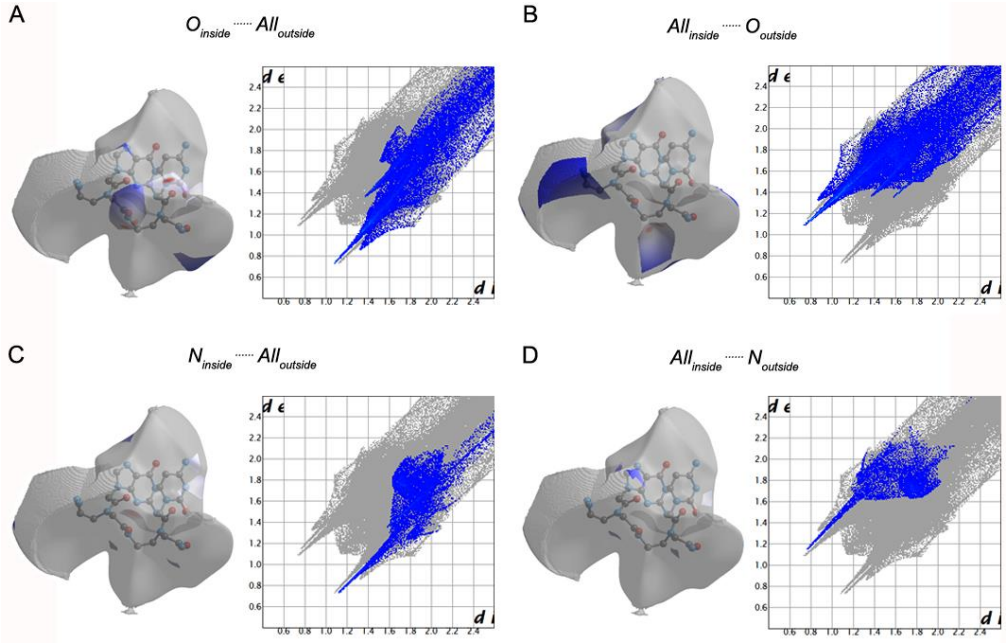

Figure S12. Hirshfeld surface and the 2-D fingerprint plot of the diPNA-**GC** supramolecular frameworks. (A) O_{inside}-$All_{outside}$, (B) All_{inside}-$O_{outside}$, (C) N_{inside}-$All_{outside}$, (D) All_{inside}-$N_{outside}$.

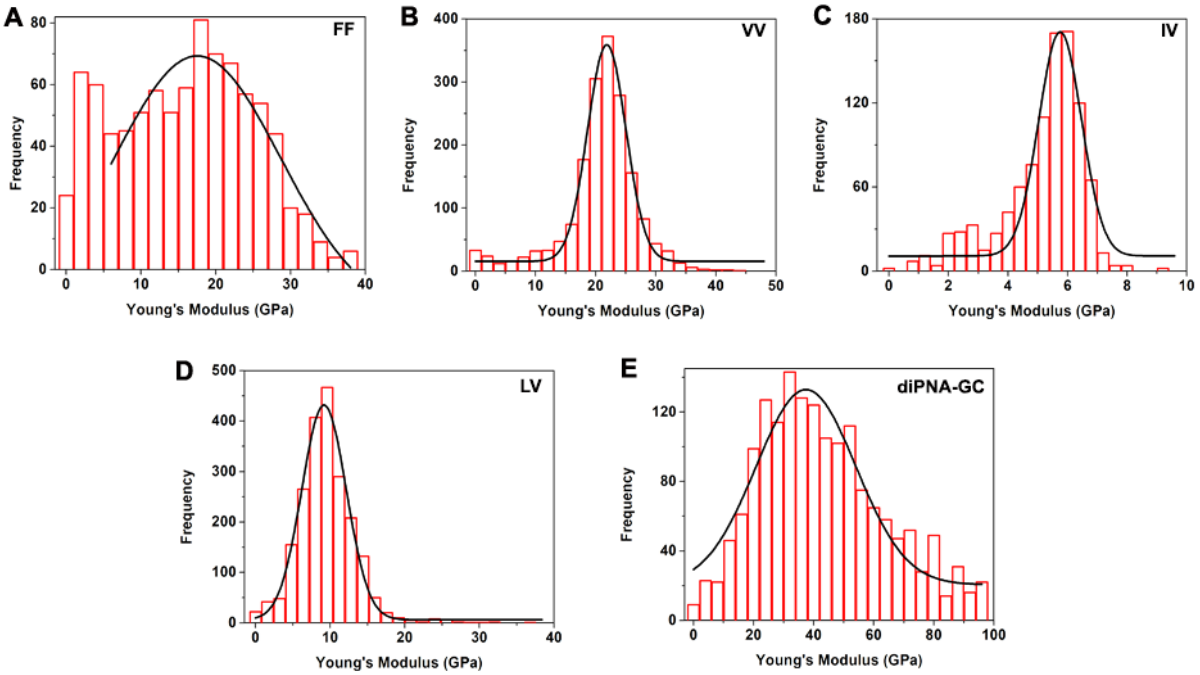

Figure S13. Statistical Young's modulus distribution of the bioinspired suprahelical frameworks self-assembled by (A) **FF**, (B) **VV**, (C) **IV**, (D) **LV** and (E) diPNA-**GC**. At least 2000 counts for each item were used for statistics.

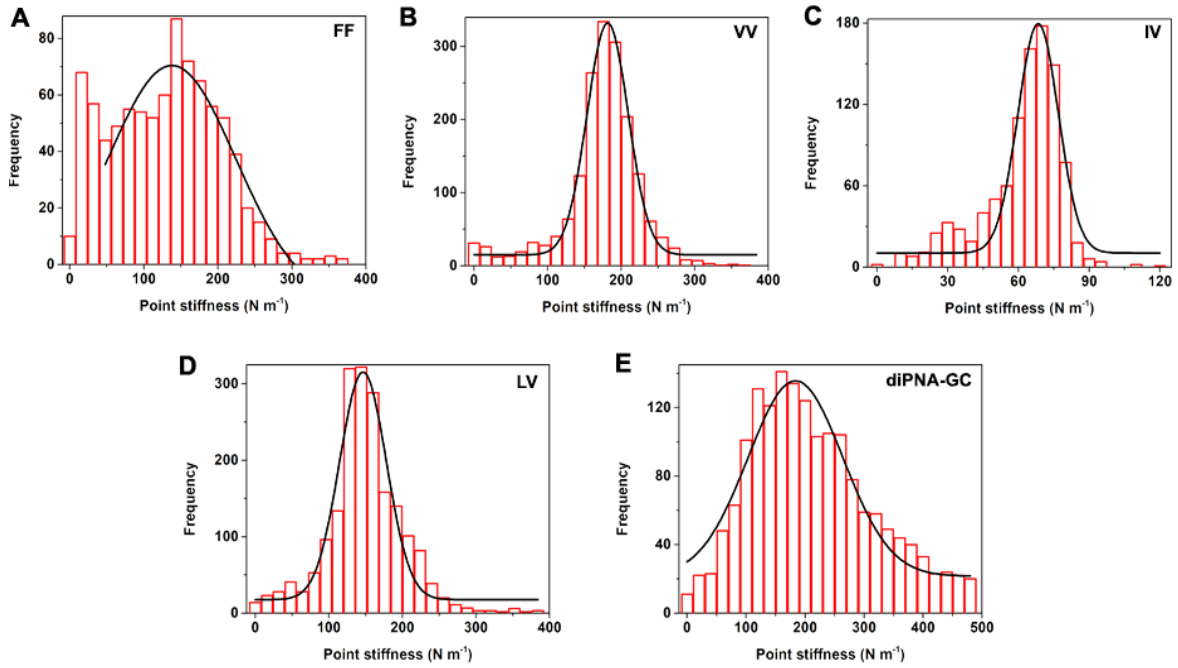

Figure S14. Statistical point stiffness distribution of the bioinspired suprahelical frameworks self-assembled by (A) **FF**, (B) **VV**, (C) **IV**, (D) **LV** and (E) diPNA-**GC**, derived from the calculated transformation of the corresponding Young's moduli.

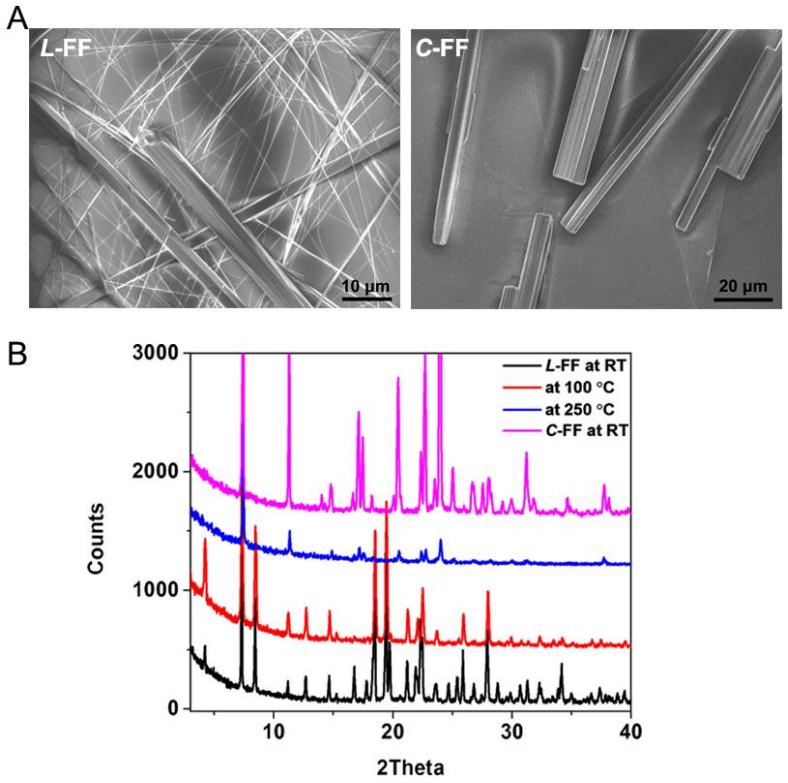

Figure S15. (A) SEM images of **FF** (*L*-**FF**) tubular and cyclo-**FF** (*C*-**FF**) platelet crystals. (B) XRD spectra showing the supramolecular phase transition from *L*-**FF** crystals to the *C*-**FF** counterparts as temperature is increased to 250 ^{o}C, thus demonstrating the thermal instability of the *L*-**FF** frameworks.

Table S2. Apparent porous parameters of the bioinspired suprahelical frameworks

Building block	**average pore diameter (nm)**	**Pore volume ($cm^3\ g^{-1}$)**	**specific surface area ($m^2\ g^{-1}$)**
FF	3.4	0.11	42.3
VV	3.1	0.03	22.1
IV	2.7	0.008	12.4
diPNA-**GC**	3.4	0.14	68.1

Note that **LV**-based frameworks show negligible data.

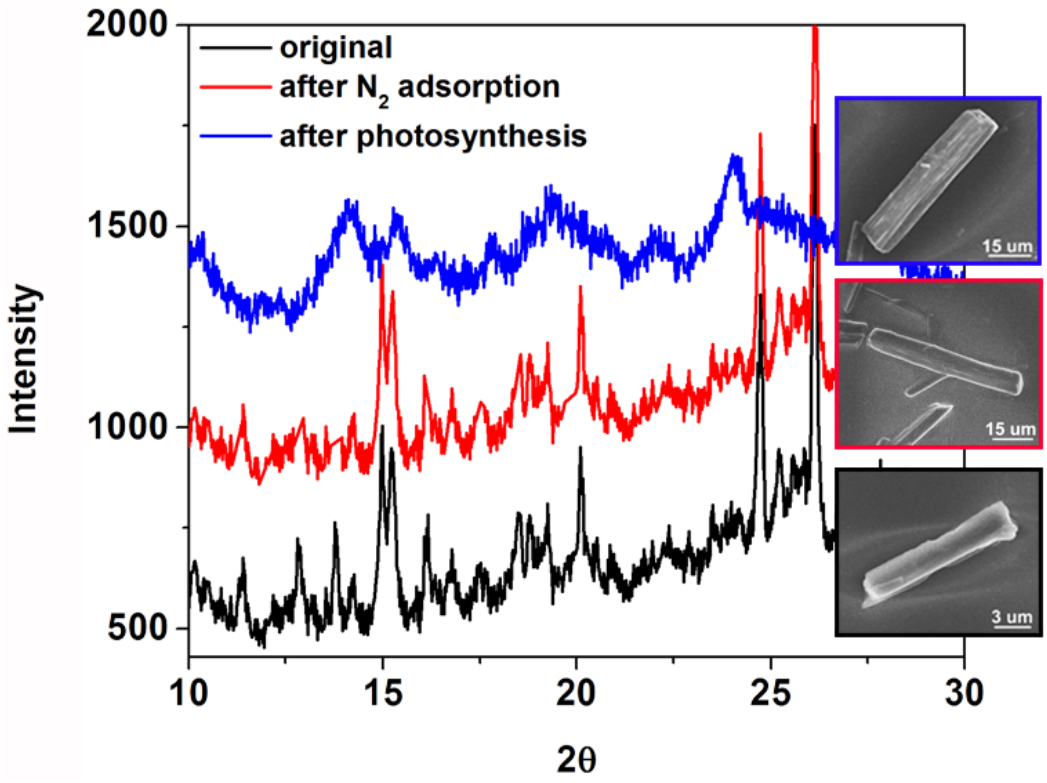

Figure S16. XRD characterizations of the original diPNA-**GC** frameworks (black), after BET experiment (red) and artificial photosynthesis experiment (blue). The insets show the SEM images of the corresponding crystals.

In spite of the low signal-to-noise ratios, the XRD and SEM characterizations of the crystals after the nitrogen adsorption and artificial photosynthesis experiments revealed the same profiles as the original ones, demonstrating the stability of the bioinspired crystals.

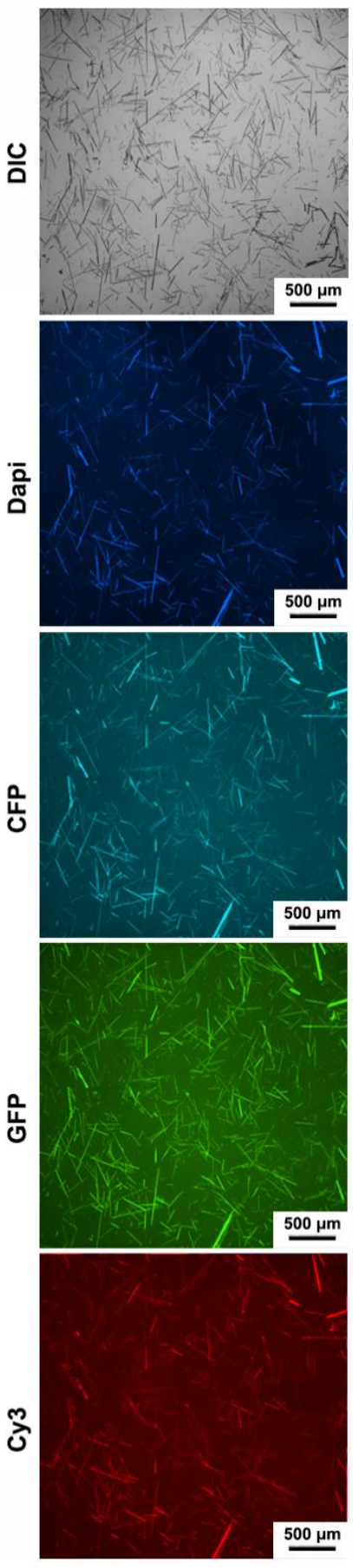
DIC
500 µm
Dapi
500 µm
CFP
500 µm
GFP
500 µm
Cy3
500 µm

Figure S17. Fluorescence microscopy images of the diPNA-**GC** self-assembling suprahelical frameworks. DIC: differential interference contract mode; Dapi: 4',6-diamidino-2-phenylindole filter (Ex: 340-380 nm, Em: 435-485 nm); CFP: cyan fluorescent protein filter (Ex: 420-445 nm, Em: 460-510 nm); GFP: green fluorescent protein filer (Ex: 455-485 nm, Em: 500-545 nm); Cy3: cyanine 3 (Ex: 528-553 nm, Em: 590-650 nm).

The results demonstrate that upon different excitations, the bioinspired suprahelical frameworks showed different emissions, thus indicating the ability of wide-spectrum photon-electron transformations.

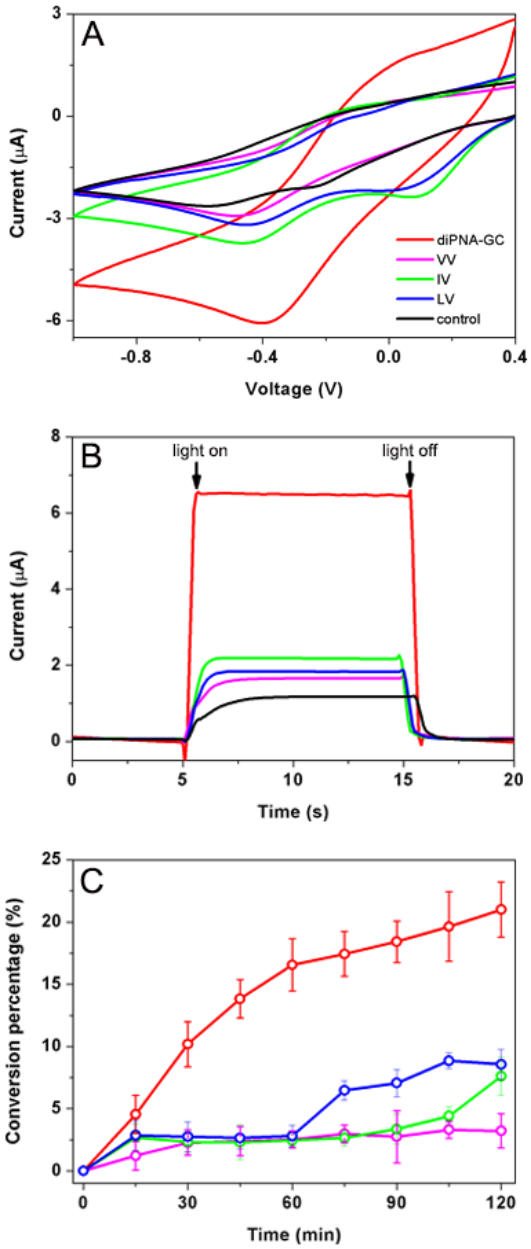

Figure S18. Comparison of the artificial photosynthesis systems using the amide-based suprahelical frameworks as scaffolds. (A) Cyclic voltammogram of $Ru(bpy)_3Cl_2$, (B) photocurrent response, and (C) conversion percentage of NADH in the presence of the artificial photosynthesis system using different suprahelical frameworks as the scaffolds, as noted in (A). In (A, B), the same experiments without the suprahelical frameworks are shown in black as controls. Note that the data of the diPNA-**GC** system were extracted from Figure 5C, D, F of the main text.

The results demonstrate that the artificial photosynthesis systems constructed employing other suprahelical frameworks with lower cavity ratios as the scaffolds showed reduced efficiency compared to diPNA-**GC**.

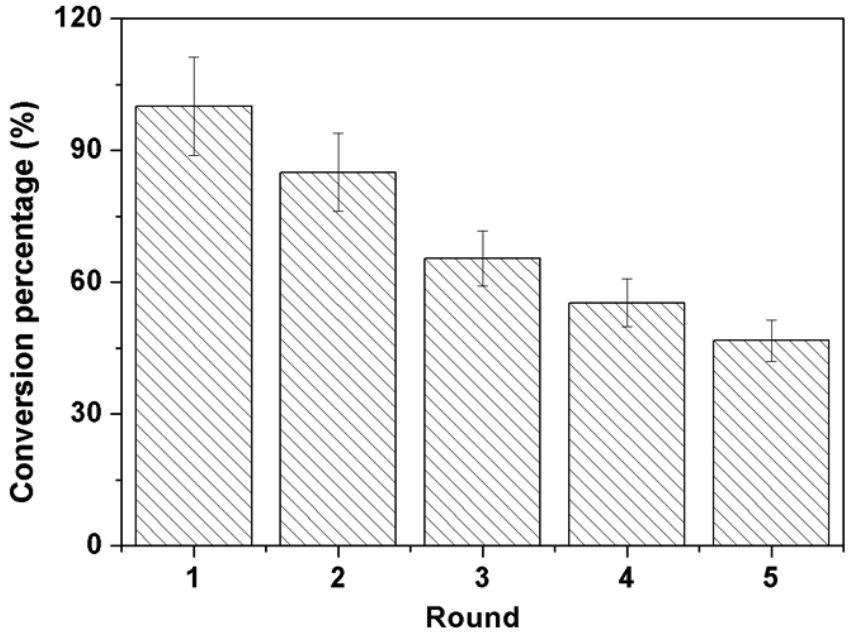

Figure S19. Cyclic conversion of NADH in the presence of the artificial photosynthesis system using diPNA-**GC** frameworks as the scaffolds.

References

(1) Görbitz, C. H. The Structure of Nanotubes Formed by Diphenylalanine, the Core Recognition Motif of Alzheimer's β-Amyloid Polypeptide. *Chem. Commun.* **2006**, 2332-2334.